COMPUTED POTENTIAL ENERGY SURFACES FOR CHEMICAL REACTIONS

Semi-Annual Report

for the period

January 1, 1992 - June 30, 1992

for
Cooperative Agreement NCC2-478

Submitted to

National Aeronautics and Space Administration
Ames Research Center
Moffett Field, California 94035

Computational Chemistry Branch
Dr. Stephen R. Langhoff, Chief and Technical Monitor

Thermosciences Division
Dr. Jim Arnold, Chief

Prepared by

ELORET INSTITUTE
1178 Maraschino Drive
Sunnyvale, CA 94087
Phone: 408 730-8422 and 415 493-4710
Telefax: 408 730-1441

Dr. K. Heinemann, President and Grant Administrator
Dr. Stephen P. Walch, Principal Investigator

25 August, 1992

The work on the NH + NO system which was described in the last progress report has been written up and a draft of the manuscript is included in the appendix. The appendix also contains a draft of a manuscript on an Ar + H + H surface which was generated in collaboration with Schwenke and Taylor.

New work which was completed in the last six months includes: i) calculations on the $^1CH_2 + H_2O$, $H_2 + HCOH$, and $H_2 + H_2CO$ product channels in the CH_3 + OH reaction, ii) calculations for the NH_2 + O reaction, iii) calculations for the $CH_3 + O_2$ reaction, and iv) calculations for CH_3O and the two decomposition channels - CH_2OH and $H + H_2CO$. Detailed descriptions of this work will be given in manuscripts; however, brief descriptions of the CH_3 + OH and CH_3 + O_2 projects are given below.

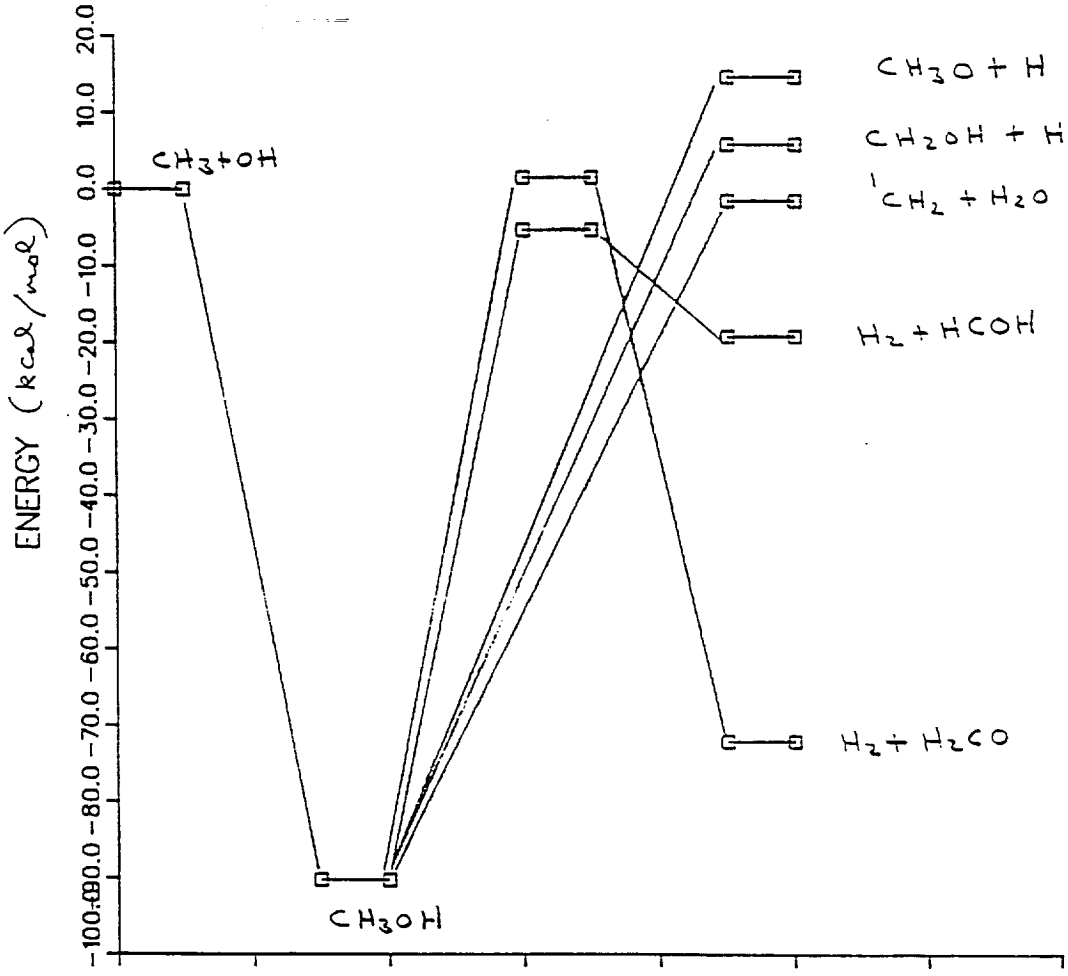

Fig. 1. Schematic of the PES for CH_3 + OH.

The decomposition channels of CH_3OH are believed to be important in hydrocarbon combustion. Researchers at Lewis research center were interested in the H + CH_3O and H + CH_2OH channels, however, at an ACS symposium (San Francisco, April 1992) it became apparent that there were other important channels specifically $^1CH_2$ + H_2O, H_2 + HCOH, and H_2 + H_2CO. There had been a previous study of this system by Harding et al. but this work was 10 years old and could be substantially improved upon with current methodology. Fig. 1 shows a schematic of the potential energy surface (PES) of this system as obtained by CASSCF/gradient plus CCI calculations. (The computational method is discussed in the HN + NO manuscript.) This PES is believed to be accurate to $\pm$ 2 kcal/mol based on comparison to the known thermochemistry of reactants and products. From the calculations, the most likely product channels are H_2 + HCOH and $^1CH_2$ + H_2O since the barriers are below the CH_3 + OH reactants. However the barrier to forming H_2 + H_2CO is only 1.7 kcal/mol (relative to CH_3 + OH). The latter barrier is considerably lower than in the Harding et al. calculations. The $^1CH_2$ + H_2O channel has no barrier. This channel is complex, involving an initial electrostatic interaction (dipole-dipole leading term), subsequent formation of a dative bond structure, followed by insertion of $^1CH_2$ into an OH bond of H_2O to give CH_3OH. The CH_3O + H, and CH_2OH + H channels are endothermic with respect to CH_3 + OH but involve no barriers. These channels could be reached at higher temperatures. The transition state geometries and frequencies and the computed energetics have been made available to G. Smith (SRI) and M. Pilling (Leeds Univ., England) for use in RRKM calculations directed toward understanding this complex and important system.

Fig. 2 shows a schematic of the PES for CH_3 + O_2. These calculations were carried out with a plane of symmetry (one CH bond in the plane formed by the C and two O atoms). With this symmetry constraint, there is a $^2A''$ surface which correlates with CH_3 plus the ground $^3\Sigma_g^-$ state of O_2 and a $^2A'$ state which correlates with CH_3 plus the $^1\Delta_g$ state of O_2. There is no entrance channel barrier on the $^2A''$ surface, but there is an entrance channel barrier on the $^2A'$ surface. This is consistent which what is known for the corresponding states of the H + O_2 system. The $^2A''$ surface leads to CH_3O + O products, with no barrier

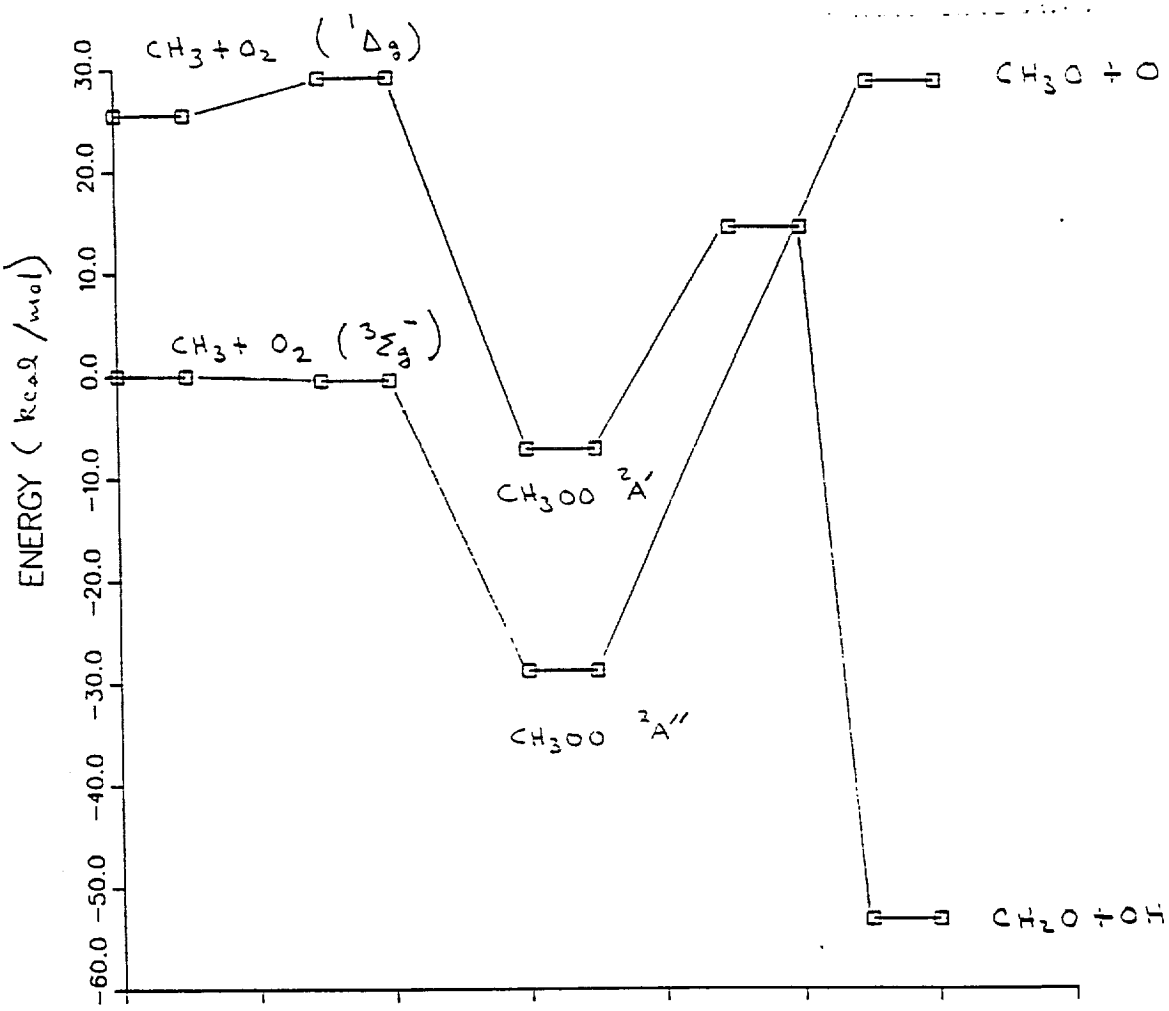

Fig. 2. Schematic of the PES for $CH_3 + O_2$.

other than the exoergicity. The $^2A'$ surface leads to $CH_2O + OH$ products via a 1,3-hydrogen shift. The barrier to this process is 14.5 kcal/mol relative to CH_3 plus O_2 $^3\Sigma_g^-$. The experimental situation for this reaction is quite uncertain. Reported activation energies range from 9.1-21.1 kcal/mol and the rate constant is uncertain by two orders of magnitude at flame temperatures. If a surface crossing between $^2A''$ and $^2A'$ is assumed, the present calculations predict an activation energy of 14.5 kcal/mol and $CH_2O + OH$ as the primary product.

Theoretical Characterization of the Potential Energy Surface for NH + NO

Stephen P. Walch[a]
ELORET Institute
Palo Alto, Ca. 94303

Abstract. The potential energy surface (PES) for NH + NO has been characterized using complete active space self-consistent field (CASSCF) gradient calculations to determine the stationary point geometries and frequencies followed by CASSCF/ internally contracted configuration interaction (CCI) calculations to refine the energetics. The present results are in qualitative accord with the BAC-MP4 calculations of Melius and Binkley, but there are differences as large as 8 kcal/mol in the detailed energetics. Addition of NH to NO on a $^2A'$ surface, which correlates with N_2 + OH or H + N_2O products, involves barriers of 3.2 kcal/mol (trans) and 6.3 kcal/mol (cis). Experimental evidence for these barriers is found in the work of Böhmer et al. The $^2A''$ surface has no barrier to addition, but does not correlate with products. Surface crossings between the barrierless $^2A''$ surface and the $^2A'$ surface may be important. Production of N_2 + OH products is predicted to occur via a planar saddle point of $^2A'$ symmetry. This is in accord with the preferential formation of $\Pi(A')$ Λ doublet levels of OH in the experiments of Patel-Misra and Dagdigian. Addition of NH $^1\Delta$ to NO is found to occur on an excited state surface and is predicted to lead to N_2O product as observed by Yamasaki et al.

[a]Mailing Address: NASA Ames Research Center, Moffett Field, CA 94035.

I. Introduction

The reaction of NH with NO is important in the combustion of nitrogen containing fuels and in the thermal De-NO_x process in which NO is converted to N_2 by the addition of NH_3 [1-4]. The latter process is important in controlling NO_x emissions from jet engines.

Considering the X $^3\Sigma^-$ ground state of NH, there are two exothermic product channels.

$$NH\ X\ ^3\Sigma^- + NO \rightarrow N_2 + OH \tag{1}$$

$$NH\ X\ ^3\Sigma^- + NO \rightarrow H + N_2O \tag{2}$$

Experimental estimates of the product branching ratio vary widely. Yamasaki et al. [5] concluded that reaction (1) accounted for 100 % of the products, while Mertens et al. [6] reported that reaction (1) accounted for only 19 $\pm$ 10 % of the products.

The PES for reaction (1) [7,8,9] involves an intermediate HNNO complex which undergoes a 1,3-hydrogen shift with a barrier to form an NNOH species which is unstable and dissociates to N_2 + OH. The HNNO complex can also dissociate over a barrier to H + NNO. The reverse process

$$H + NNO \rightarrow N_2 + OH \tag{3}$$

$$H + NNO \rightarrow NH + NO \tag{4}$$

has also been studied. Reaction (3) can occur via a direct process in which H attaches to the O end of N_2O, or via an indirect process in which the H attaches to the end N of N_2O and then undergoes a 1,3-hydrogen shift leading to products via the same saddle point as for reaction (1) [8].

The internal energy distribution of the OH product for reaction (1) has been studied by Patel-Misra and Dagdigian [10] in a crossed beam experiment. The OH v=1 to v=0 vibrational population ratio was found to be 0.30 ± 0.06 and the average rotational energy was found to be 25 ± 1 kJ/mol (5.97 ±0.23 kcal/mol). These authors note that this is a rather small amount of internal excitation given that reaction (1) is exothermic by 408 kJ/mol (97.5 kcal/mol). Attempts to model the internal energy distribution in the OH product by phase space theory lead to more excitation than observed, suggesting that the HNNO complex may not be long enough lived to exhibit statistical behaviour. In this study the internal energy distribution in the N_2 was not measured and it was presumed that most of the excess energy went into relative translational energy of the products. More recently, Böhmer et al. [11] have studied the reaction of N_2O with hot H atoms formed by photolysis of an N_2O-HI complex. This study is in general agreement with the work of Patel-Misra and Dagdigian with respect to the OH internal energy distribution, but the OH Doppler shift profiles in these experiments require a large amount of internal vibrational excitation of the N_2 ($\approx$ 25,000 cm^{-1} (71.5 kcal/mol) for OH v=0). This result is explained by a model in which the HNNO complex has an elongated NN bond and the 1,3-hydrogen shift is assumed to occur rapidly with respect to motion of the heavy atoms leaving the N_2 product vibrationally excited. A more detailed understanding of the product energy distributions and branching ratios in this system requires more detailed information about the PES, which is reported in this paper.

Unlike many other reactions of NH, where the $^1\Delta$ state is more reactive, the NH + NO reaction is found to have comparable rates for the ground $X^3\Sigma^-$ state and the low lying $^1\Delta$ state of NH [5]. Yamasaki et al. [5] find a strong product specificity depending on the NH spin state. The ground state of NH leads to N_2 + OH as the

predominant product, while the $^1\Delta$ state of NH also leads to H + N_2O. In addition, NO is able to quench NH $^1\Delta$ to NH $^3\Sigma^-$.

$$NH\ ^1\Delta + NO \rightarrow H + N_2O \tag{5}$$

$$NH\ ^1\Delta + NO \rightarrow NH\ X\ ^3\Sigma^- + NO \tag{6}$$

In the work of Yamasaki et al. the experimental results are analyzed in terms of a model based on a calculated PES by Melius and Binkley [7] and Fueno et al. [9]. In this picture NH ($^1\Delta$) + NO correlates with a $^2A'$ surface which also correlates with H + N_2O, while NH (X $^3\Sigma^-$) + NO correlates with a HNNO complex on the $^2A''$ surface. As discussed below, this model is substantially oversimplified. In fact NO + NH in the $^3\Sigma^-$ and $^1\Delta$ state lead to six surfaces which are strongly coupled and the reaction of the $^1\Delta$ state of NH is a carbene insertion process which occurs on an excited state surface. Preliminary calculations on the excited state surfaces are also reported here.

There have been several previous studies of the PES for NH + NO. The most extensive of these is by Melius and Binkley [7] and used the BAC-MP4 method with a 6-31G** basis set. More recently Fueno et al.[9] have also carried out multi reference configuration interaction (MRCI) studies of this system using smaller basis sets. The present calculations are similar in spirit to these earlier studies, but use larger basis sets and more extensive configuration interaction. Thus, the present results are expected to be more reliable than the earlier studies. Qualitative features of the potential energy surfaces are discussed in Sec. II, the computational method is discussed in Sec. III, the results are presented in Sec. IV, and the conclusions are given in Sec. V.

II. Qualitative Features.

Combining the $^3\Sigma^-$ ground state of NH with the $^2\Pi$ ground state of NO and keeping a plane of symmetry leads to $^{2,4}A'$ and $^{2,4}A''$ surfaces. (It should be noted here that for four atoms the reaction may occur without symmetry; however, the key stationary points on the surface are found to have C_s symmetry and this symmetry is assumed in the following discussion.)

For the $^2A''$ surface, the singly occupied NO 2π orbital is in the plane of the supermolecule and addition of NH to NO occurs with no barrier.

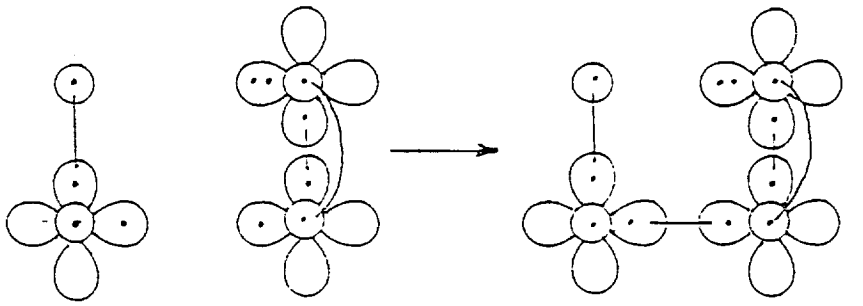

(7)

However, a doubly occupied O 2p orbital is in the plane of the supermolecule and 1,3-hydrogen migration is unfavorable. Thus, approach on this surface would not be expected to lead to N_2 + OH products. Also this surface can not lead to H + N_2O, since this product channel is of $^2A'$ symmetry.

For the $^2A'$ surface, the singly occupied NO 2π orbital is perpendicular to the plane of the supermolecule and the NH is adding to an NO π bond. Thus, a barrier to addition is expected on this surface. However, a singly occupied O 2p orbital is in the plane of the supermolecule and 1,3-hydrogen migration leading to NNOH may occur. This process is expected to have a barrier since an NH bond is being broken as the OH bond is formed. The NNOH species is not bound and the 1,3-hydrogen migration leads directly to N_2 + OH.

Fig. 1 shows a schematic of the potential energy surface for NH + NO. Focusing

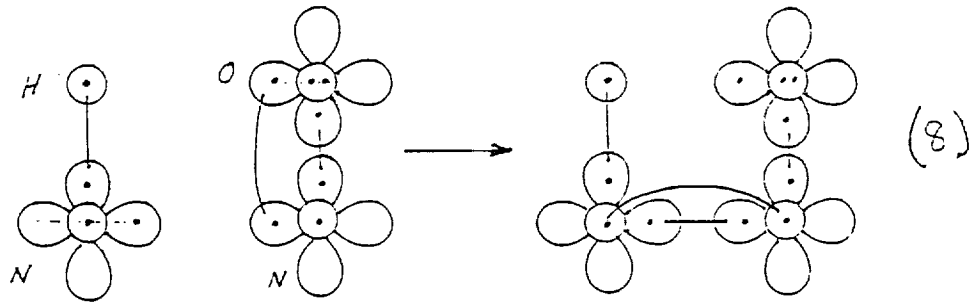

(8)

first on the features discussed above, it is seen that NH + NO may form HNNO in the cis or trans orientation with no barrier on the $^2A''$ surface, but there are barriers on the $^2A'$ surface. HNNO corresponds to a stable planar minimum on the PES and the $^2A'$ state is lower than the $^2A''$ state. This leads to entrance channel surface crossings between these two surfaces, which may lead to surface hopping between the $^2A''$ surface, which forms with no barrier, and the $^2A'$ surface, which has an entrance channel barrier but leads to products. cis-HNNO on the $^2A'$ surface may undergo a 1,3-hydrogen shift leading to N_2 + OH products.

From Fig. 1 it is also seen that H + NNO correlates with the $^2A'$ surface. Addition of H to the O end of N_2O leads directly to N_2 + OH with a large barrier. An alternative indirect pathway involves addition of H to the end N of N_2O which leads to cis-HNNO with a smaller barrier than addition to the O end. This pathway then connects to N_2 + OH by the same 1,3-hydrogen shift saddle point involved in the NH + NO reaction. The indirect pathway has a lower overall barrier and should be the predominate pathway at lower temperatures.

Addition of the low-lying $^1\Delta$ excited state of NH to NO involves a geometry in which the N atom of NH approaches near the midpoint of the NO bond with the NH bond approximately perpendicular to the plane formed by the N atom of NH and the NO bond. Combining the $^3\Sigma^-$ and $^1\Delta$ states of NH with the $^2\Pi$ state of

NO leads to six potential energy surfaces. Of these the lowest two are the $^2A'$ and $^2A''$ surfaces which correlate with the $^3\Sigma^-$ ground state of NH. Of the remaining four surfaces three are repulsive and one is attractive. The electronic configuration of the attractive state is:

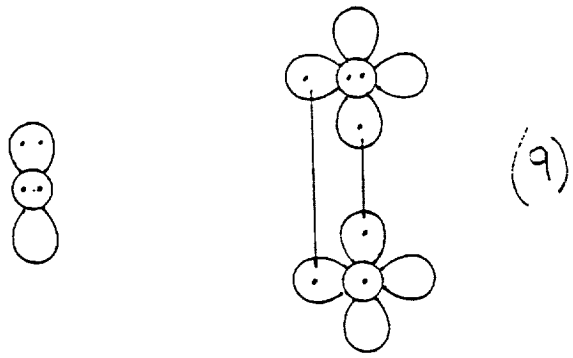

(9)

(where the doubly occupied N 2p orbital perpendicular to the plane represents the NH bond pair of NH) This configuration is analagous to the configuration involved in insertion of $O(^1D)$ into H_2 [12]. This configuration can also correlate with H + N_2O, since dissociation of the NH bond leads to a configuration with four a' and four a'' (with respect to the NNO plane) electrons in π orbitals on the N_2O. It is probable that this excited surface accounts for the production of N_2O observed by Yamasaki et al. [5] in the reaction of NH $^1\Delta$ with NO.

III. Computational Details.

Two different basis sets were used in this work. For the CASSCF gradient calculations the polarized double zeta set of Dunning and Hay [13] was used. The basis set for N and O is a (9s5p)/[3s2p] basis augmented by a single set of 3d functions with exponents of 0.80 and 0.85 for N and O, respectively. The H basis is (4s)/[2s] augmented with a single set of 2p functions with exponent 1.00. The basis set used in the CI calculations is the Dunning correlation consistent triple zeta double polarization basis set [14]. This basis is [4s3p2d1f] for N and O and [3s2p1d] for H

and is described in detail in Ref. 14.

The CASSCF calculations had 13 electrons distributed among 8 a′ and 3 a″ orbitals. The active electrons correspond to the electrons depicted in Eqns. 7 and 8 plus the 2s electron pair on the central N. The remaining 10 electrons are the two pairs of N 1s electrons, the O 1s and 2s electron pairs, and the N 2s electron pair on the end N. One N 2s pair has to be active to describe certain regions of the surface (e.g. H + N_2O) where the N 2s electrons on the central N are used in bonding.

All but the N 1s and O 1s electrons are correlated in the subsequent CCI calculations. A selected reference list was used with a coefficient cutoff of 0.04.

The CASSCF/gradient calculations used the SIRIUS/ABACUS system of programs [15], while the CCI calculations were carried out with MOLPRO [16,17]. Most of the calculations were carried out on the NASA Ames Cray Y-MP. Some of the CCI calculations were carried out on the NAS facility YMP.

IV. Discussion.

Before discussing the results for the HN + NO reaction, it is useful to consider results for the molecular species involved. Table I compares geometries and harmonic vibrational frequencies from CASSCF/gradient calculations for NH, NO, N_2O, OH, and N_2 with experiment. The results shown in Table I are typical of results obtained at stable minimum points on a PES using CASSCF/gradient methods. Here it is seen that the bond lengths are too long by ≈ 0.02 $\AA$ but the vibrational frequencies are in fair agreement with experiment. This result contrasts with the results of Hartree-Fock theory, which typically gives bond lengths which are somewhat shorter than experiment and frequencies which are larger than experiment. It has been common practice to scale SCF frequencies by ≈ 0.9 to account for this defect in the SCF results. The CASSCF frequencies on the other hand are approximately correct and are used here without scaling.

Tables IIa and IIb show comparisons of CASSCF/gradient and externally contracted CI [18] calculations for the HN_2 and HO_2 surfaces. Once again at the minima on the PES's, corresponding to HN_2 and HO_2, the geometries and frequencies are in fair agreement with the more accurate CCI results. (The bond lengths from the CASSCF calculations are slightly too long as noted above.) At the saddle points the CASSCF results are poorer. In both cases the saddle point geometry is tighter in the CASSCF calculations than in the CCI calculations, as evidenced by a shorter HN/HO bond length, a larger bending frequency, and a larger imaginary frequency at the saddle point. It is also seen from Table II that the binding energies are smaller in the CASSCF calculations. These results are typical, based on experience with other systems. For HN_2 it has been shown that addition of a correction term, which is a slowly varying function of the NH bond length, to the CASSCF surface results in a reasonable approximation to the CCI surface [19]. This result suggests that the CASSCF surface is mainly distorted along the reaction coordinate, but is a better representation in the directions orthogonal to the reaction coordinate. Thus, one way to correct the CASSCF surface near a saddle point would be to compute CI energies along the minimum energy path on the CASSCF surface. This approach has actually been carried out for the reaction of $^1CH_2$ + H_2O [20], which is a barrierless process. However, for the present system the saddle points involve barriers and are expected to be less sensitive to small changes of the geometry along the reaction coordinate. Thus, the approach used here is to carry out CCI calculations at the stationary point geometries obtained at the CASSCF level.

Tables IIIa and IIIb give computed frequencies and geometries for the $^2A'$ and $^2A''$ states of HNNO, respectively. Table IV gives the computed CCI energies at each of the stationary points, the zero-point energies, and the relative energies (

including zero-point energy). The same energetics are shown graphically in Fig. 1.

From Table IIIa it is seen that addition of NH to NO on the $^2A'$ surface occurs with loose saddle points i.e. the bond lengths and frequencies are close to those for NH and NO. The saddle points for adding H to the end N and O of N_2O show somewhat more distortion of bond lengths, r_{NN} elongated by 0.03 $\AA$ for H-NNO and r_{NO} elongated by 0.07 $\AA$ for NNO-H.

Cis and trans HNNO on the $^2A'$ surface have similar bond lengths. Both the NN and NO bond lengths of HNNO on the $^2A'$ surface are shorter than on the $^2A''$ surface. The NN bond length is shorter by 0.10 $\AA$ and 0.12 $\AA$ for cis and trans HNNO, respectively. This effect results from the greater NN π bonding on the $^2A'$ surface which is evident from Eqn's (7) and (8). The shorter NO bond on the $^2A'$ surface is probably due to smaller non-bonded repulsions between the doubly occupied O 2p orbital and the NN bond orbitals.

The saddle point for 1,3-hydrogen migration in cis-HNNO leading to N_2 + OH product (denoted NNOH in Table IIIa), by contrast with the other saddle points discussed above, would be described as a tight saddle point. Here the NN bond is elongated by 0.11 $\AA$ (compared to a comparable N_2 calculation, Table I). As discussed by Böhmer et al. [11] (see section I), this elongation of the NN bond is believed to be responsible for the production of vibrationally excited N_2 product.

Table V compares the geometries and frequencies obtained in the present calculations with the BAC-MP4 results of Melius and Binkley [7,21]. It should be noted that the frequencies reported by Melius and Binkley have been scaled downward by 12 %. For cis-HNNO the CAS bond lengths are somewhat longer than those obtained with the BAC-MP4 method. This is expected from the discussion above. The frequencies are in fair accord but there appears to be a tendency for the CAS frequencies to be larger than the scaled UHF frequencies. For the saddle points the

CASSCF geometries are again in reasonable accord with the UHF geometries (taking into account the tendency for CAS to slightly overestimate bond lengths). One interesting difference is that CAS leads to a larger imaginary frequency for NNO-H compared to NNOH, while UHF shows the opposite trend. This could have some significant dynamical consequences, because in Ref. 8 a one dimensional tunneling correction was made based on the imaginary frequency.

Table VI compares the CAS/CCI energetics with those obtained using the BAC-MP4 method. Here there is sporadic agreement. In particular, the NNO-H and NNOH saddle point energies agree to within 2 kcal/mol with the present calculations, but the H-NNO saddle point is 6.7 kcal/mol lower in the present calculations. A peculiar result is that the BAC-MP4 calculations find cis-HNNO below trans-HNNO which is the opposite of what is found in the present calculations. It should be noted here that the BAC-MP4 method makes rather large corrections ($\approx$ 10 kcal/mol for single bonds and $\approx$ 20 kcal/mol for double bonds) to the energies. The present calculations use no empirical corrections yet yield results of at least as good accuracy. The incorrect ordering for cis and trans HNNO is puzzling because the correct ordering is obtained with CASSCF and CCI. Still the present results tend to support the utility of the BAC-MP4 method, though the present large scale CI calculations are undoubtedly more reliable.

We now turn to a more detailed discussion of the computed potential energy surface as shown in Fig. 1 and based on the energetics given in Table IV. As shown in Fig. 1 there are barriers to the addition of NH to NO on the $^2A'$ surface. The computed barrier heights are 6.3 kcal/mol for cis approach and 3.2 kcal/mol for trans approach. These barriers are expected based on the discussion in Section II and are similar in origin to barriers for addition of H to NO [22]. Experimental verification of these barriers is obtained in experiments of Böhmer et al. [11] which

measure the threshhold for formation of NH $^3\Sigma^-$ in the reaction of hot H atoms with NO formed by photolysis of an HI-NO complex. These experiments indicate a threshhold occuring for a photolysis wavelength between 250 and 260 nm whereas the energy of the lowest vibrational level of NH $^3\Sigma^-$ + NO occurs at $\approx$ 270 nm, a difference of $\approx$ 4-9 kcal/mol. It should be noted here that H + NO correlates with the $^2A'$ surface and dissociation to NH + NO therefore should involve a barrier.

Addition on the $^2A''$ surface involves no barrier but this surface does not correlate with H + N_2O nor, from the discussion in Section II, is it likely to lead to OH + N_2 products. Because the $^2A'$ surface drops more rapidly than the $^2A''$ surface, surface crossings are expected in the NH + NO entrance channel region. These surface crossings may allow addition to occur on the barrierless $^2A''$ surface with subsequent surface crossing to the $^2A'$ surface which connects to products. This process could reconcile the apparent lack of a barrier to reaction (1) with the expectation that the products pass through the planar NNOH saddle point, which has $^2A'$ symmetry. Evidence that the products arise via a saddle point of $^2A'$ symmetry comes from the experiments of Petel-Misra and Dagdigian [10] in which a marked preference for $\Pi(A')$ Λ doublet levels is observed in the OH product.

The reverse reaction of H + N_2O i.e reactions (3) and (4) has been studied by Marshall et al. [8] and by Böhmer et al. [11]. The present results are consistent with the discussion in Ref. 8. The production of N_2 + OH can proceed via a direct process in which the H adds to the O end of N_2O. The computed barrier height for the direct pathway is 18.0 kcal/mol. The indirect pathway involves addition of H to the end N of N_2O which has a 10.3 kcal/mol barrier and a subsequent 1,3-hydogen shift to yield products via the NNOH saddle point which has a 16.3 kcal/mol barrier. Thus, the indirect pathway has a lower overall barrier and should be the more favorable process at lower temperatures.

The reaction of the $^1\Delta$ excited state of NH with NO, reaction (5), has also been studied. The reaction of NH $^1\Delta$ with H_2 has been studied by Fueno et al. [23]. These authors observed an initial approach geometry in which the N atom approaches perpendicular to the midpoint of the H_2 bond and the NH bond is perpendicular to the plane formed by the N and H_2 molecule. Fig. 2 shows the electronic structure for the lowest six surfaces of NH + NO for this geometric arrangement. Two of these surfaces arise from the $^3\Sigma^-$ state of NH and the remaining four surfaces arise from the $^1\Delta$ state of NH. Of these surfaces the one which allows insertion is given by Eqn. (9). A limited study of this insertion process was made using a state averaged CASSCF calculation (averaged over the six lowest roots) varying only the N to NO bond midpoint distance (R) as shown in Fig. 3. From Fig. 3 curve crossings are evident between the diabatic states arising from NH $^3\Sigma^-$ state (repulsive) and the diabatic state arising from Eqn (9). If the H atom is allowed to dissociate from the initially formed HN-NO adduct, there are four electrons of π' and four electrons of π'' symmetry with respect to the NNO plane. Thus, this structure does correlate with the ground state of N_2O and it is plausable that production of N_2O via addition of NH $^1\Delta$ to NO occurs via the third excited surface.

V. Conclusions.

The potential energy surface for NH + NO has been characterized using CASSCF gradient calculations to determine the stationary point geometries and frequencies followed by CASSCF/ internally contracted CI calculations to determine the energetics. The CASSCF method is found to give reasonable geometries and frequencies at minima on the PES. At saddle points the geometries and frequencies are somewhat less accurate as revealed by comparison of CASSCF and CCI results for the HN_2 and HO_2 PES's. Studies of the HN_2 PES indicate that the CASSCF surface is distorted from the more accurate CCI surface mainly in the direction of the re-

action coordinate, while directions orthogonal to the reaction coordinate are better represented.

In general the present results are in qualitative accord with the work of Melius and Binkley using the BAC-MP4 method. However, the present calculations have no empirical corrections while the BAC-MP4 method involves large corrections ($\approx$ 10 kcal/mol for single bonds and $\approx$ 20 kcal/mol for multiple bonds). There are also some large discrepancies (as large as 8 kcal/mol) in detailed energetics between the present work and the BAC-MP4 results.

Addition of NH to NO on a $^2A''$ surface involves barriers of 3.2 kcal/mol for trans orientation and 6.3 kcal/mol for cis orientation. The presence of these barriers is predicted from simple qualitative considerations and is supported experimentally by threshhold measurements for production of NH + NO in the reaction of hot H atoms formed by photolysis of an HI-NO complex in the experiments of Böhmer et al.

Production of N_2 + OH products is predicted to occur via a 1,3-hydrogen shift from an initially formed cis HNNO adduct of planar $^2A'$ symmetry. This conclusion is supported by experiments of Petel-Misra and Dagdigian in which a marked preference for $\Pi(A')$ Λ doublet levels is observed in the OH product.

Addition of NH $^1\Delta$ to NO is shown to occur on an excited state surface and to involve a geometry in which the NH approaches the NO with the N perpendicular to the NO bond midpoint and with the NH bond perpendicular to the NO-N plane. The electronic structure of this complex correlates with H plus the ground state of N_2O. This suggests that N_2O observed as the primary product in the reaction of NH $^1\Delta$ with NO by Yamasaki et al. occurs on this excited state surface.

ACKNOWLEDGMENTS

S.P. Walch was supported by a NASA grant(NCC2-478). The author thanks E.

Böhmer and P.J. Dagdigian for preprints of their work. Helpfull discussions with Carl Melius, Peter Taylor, and Curt Wittig are gratefully acknowledged.

References

1. J.A.Miller, M.C. Branch, and R.J. Kee, Combust. Flame, **43**, 81(1981).
2. R.K. Lyon, Sandia Laboratories Report No. SAND70-8635, 1970.
3. R.K. Lyon, U.S. Patent 3,900,544, August 1975.
4. R.K. Lyon, Int. J. Chem. Kinet., **8**, 315(1976).
5. K. Yamasaki, S. Okada, M. Koshi, and H. Matsui, J. Chem. Phys. , **95**, 5087(1991).
6. J.D. Mertens, A.Y. Chang, R.K. Hanson, and C. Bowman, Int. J. Chem. Kinet., **23**, 173(1991).
7. C.F. Melius and J.S. Binkley, In Proceedings of the 20th Symposium (International) on Combustion, The Combustion Institute: Pitsburg, Pa, 1984, p.575.
8. P. Marshall, A. Fontijn, and C.F. Melius, J. Chem. Phys., **86**, 5540(1987).
9. T. Fueno, M. Fukuda, and K. Yokoyama, Chem. Phys. **124**, 265(1988).
10. D. Patel-Misra and P.J. Dagdigian, J. Phys. Chem., **96**, 3232(1992).
11. E. Böhmer, S.K. Shin, Y. Chen, and C. Wittig, to be published
12. S.P. Walch and L.B. Harding, J. Chem. Phys., **88**, 7653(1988).
13. T.H. Dunning,Jr and P.J. Hay in Methods of Electronic Structure Theory, H.F. Schaefer III ed., Plenum Publishing, 1977
14. Dunning ANO's
15. SIRIUS is an MCSCF program written by H.J. Jensen and H. Agren and ABACUS is an MCSCF derivatives program written by T. Helgaker, H.J. Jensen, P. Jørenson, J. Olsen, and P.R. Taylor.
16. H.-J. Werner and P.J. Knowles, J. Chem. Phys., **89**, 5803(1988).

17. P.J. Knowles and H.-J. Werner, Chem. Phys. Lett., **145**, 514(1988).

18. P.E.M. Siegbahn, Int. J. Quantum Chem., **23**, 1869(1983).

19. S.P. Walch, unpublished results

20. S.P. Walch, to be published

21. C.F. Melius, private communication

22. S.P. Walch and C.M. Rohlfing, J. Chem. Phys., **91**, 2939(1989).

23. T. Fueno,V.B-Koutecky', and J. Koutecky', J. Am. Chem. Soc., **105**, 5547(1983).

Table I. Computed geometries and frequencies for fragments[a].

		calc.	exp.
NH	r_{NH}	1.062	1.038
	ω	3131	3282.09
NO	r_{NO}	1.174	1.1508
	ω	1889	1904.3
N_2O	r_{NN}	1.149	1.1282
	r_{NO}	1.204	1.1842
	ω_1	2267	2223.7
	ω_2	1297	1276.5
	ω_3	568(2)	589.2
OH	r_{OH}	0.988	0.9706
	ω	3624	3735.21
N_2	r_{NN}	1.123	1.0977
	ω	2315	2358.027

[a] bond lengths in $\AA$ and frequencies in cm^{-1}.

Table IIa. Comparison of CASSCF and CCI for HO_2[a]

	H-O_2		HO_2	
	CAS/grad	CCI	CAS/grad	CCI
r_{OH}	3.55	4.14	1.86	1.84
r_{OO}	2.33	2.29	2.58	2.52
$\angle$ HOO	116	116	102	104
ω_1	596 i	412 i	3617	3531
ω_2	1503	1515	1438	1417
ω_3	501	354	1058	1220
E	1.9	0.4	-39.9	-51.2

[a] Bond lengths in a_0, angles in degrees, frequencies in cm^{-1}, and E in kcal/mol.

Table IIb. Comparison of CASSCF and CCI for HN_2[a]

	H-N_2		HN_2	
	CAS/grad	CCI	CAS/grad	CCI
r_{NH}	2.49	2.64	2.05	2.02
r_{NN}	2.19	2.17	2.27	2.25
$\angle$ HNN	116	123	114	115
ω_1	1788 i	1387 i	2577	2577
ω_2	2004	2027	1735	1931
ω_3	892	668	1116	1106
E	27.4	15.8	23.6	5.6

[a] Bond lengths in a_0, angles in degrees, frequencies in cm^{-1}, and E in kcal/mol.

Table IIIa. Computed frequencies and geometries (^{2}A′ surface) [a].

	HN+NO	cis HN-NO	trans HN-NO	H+N2O	H-NNO	cis HNNO
r_{NH}	1.06	1.06	1.06		1.47	1.05
r_{NN}		1.92	1.94	1.15	1.18	1.27
r_{NO}	1.17	1.18	1.18	1.20	1.21	1.23
∠ HNN		94.4	91.7		109.6	106.5
∠ NNO		117.3	120.0	180.0	160.2	134.8
ω_1	3131	3132	3190	2267	2033	3160
ω_2	1889	1738	1791	1297	1259	1630
ω_3		778	781	568	585	1373
ω_4		282	321	568	464	1201
ω_5		732 i	687 i		1724 i	549
ω_6		468	529		604	771
trans HNNO		NNO-H		NNOH		
r_{NH}	1.04	r_{OH}	1.41	r_{NH}	1.27	
r_{NN}	1.28	r_{NN}	1.16	r_{NN}	1.23	
r_{NO}	1.22	r_{NO}	1.27	r_{NO}	1.47	
				r_{OH}	1.38	
∠ HNN	103.9	∠ HON	112.4	∠ HNN	89.9	
∠ NNO	129.6	∠ NNO	151.0	∠ NNO	95.2	
				∠ NOH	76.7	
				∠ OHN	98.1	
ω_1	3311		1989		2035	
ω_2	1628		1132		1587	
ω_3	1382		860		890	
ω_4	1228		474		467	
ω_5	589		2212 i		1934 i	
ω_6	797		556		948	

[a] Bond lengths in $\AA$, angles in degrees, frequencies in cm^{-1}.

Table IIIb. Computed frequencies and geometries ($^2A''$ surface) [a].

	cis HNNO	trans HNNO
r_{NH}	1.06	1.05
r_{NN}	1.37	1.40
r_{NO}	1.27	1.25
$\angle$ HNN	104.6	102.2
$\angle$ NNO	111.8	109.1
ω_1	3188	3274
ω_2	1437	1464
ω_3	1233	1241
ω_4	736	741
ω_5	522	491
ω_6	550	394

[a] Bond lengths in $\AA$, angles in degrees, frequencies in cm^{-1}.

Table IV. Computed energies and zero-point corrections.

	Energy	zero-point energy	Δ E
NH+NO	-184.81050(-.85245)	0.01143	0.0
H+NNO	-184.85597(-.90221)	0.01071	-31.7
cis HN-NO	-184.78351(-.84556)	0.01457	6.3
trans HN-NO	-184.78893(-.85093)	0.01507	3.2
cis HNNO	-184.87106(-.93448)	0.01979	-46.2
trans HNNO	-184.87834(-.94352)	0.02036	-51.5
NNO-H	-184.80993(-.87431)	0.01142	-13.7
H-NNO	-184.82843(-.88698)	0.01189	-21.4
NNOH	-184.81960(-.87912)	0.01350	-15.4
cis HNNO ^{2}A$''$	-184.83465(-.89268)	0.01746	-21.5
trans HNNO ^{2}A$''$	-184.83635(-.89190)	0.01732	-21.1

Table V. Comparison of BAC-MP4 and CASSCF/CCI for NH + NO; Geometries and Frequencies[a]

	cis HNNO			NNO-H			NNOH	
	CAS	UHF		CAS	UHF		CAS	UHF
r_{NH}	1.06	1.01	r_{OH}	1.41	1.52	r_{NH}	1.27	1.29
r_{NN}	1.27	1.23	r_{NN}	1.17	1.13	r_{NN}	1.23	1.20
r_{NO}	1.23	1.21	r_{NO}	1.27	1.23	r_{NO}	1.47	1.42
∠ HNN	106.5	109	∠ HON	112.4	114	r_{OH}	1.38	1.34
∠ NNO	134.8	132	∠ NNO	151.0	148	∠ HNN	89.9	90
ω_1	3160	3210	ω_1	1989	1641	∠ NNO	95.2	96
ω_2	1630	1463	ω_2	1132	1057	∠ NOH	76.7	79
ω_3	1373	1294	ω_3	860	639	∠ OHN	98.1	95
ω_4	1201	1042	ω_4	474	352	ω_1	2035	1767
ω_5	549	312	ω_5	2212 i	1559 i	ω_2	1587	1280
ω_6	771	843	ω_6	556	504	ω_3	890	958
						ω_4	467	481
						ω_5	1934 i	2427 i
						ω_6	948	807

[a] Bond lengths in Å, angles in degrees, frequencies in cm^{-1}.

Table VI. Comparison of BAC-MP4 and CASSCF/CCI for NH + NO; Energetics

Stationary Point	BAC-MP4[a,b]	CASSCF/CCI[a,c]
$H + N_2O$	0.0	0.0
NNO-H	19.8	18.0
H-NNO	3.6	10.3
[NNOH]	16.7	16.3
cis HNNO $^2A'$	-14.5	-14.5
trans HNNO $^2A'$	(-11.6)	-19.8

[a] relative energy in kcal/mol.

[b] 6-31G** basis set

[c] [4s3p2d1f/3s2p1d] basis set

Figure Captions.

Fig. 1. Schematic of the potential energy surface for NH + NO. The stationary point geomtries and vibrational frequencies are obtained at the CASSCF level, while the computed energetics are from CI calculations (See the text.). A region of crossing between $^2A'$ and $^2A''$ surfaces in the NH + NO entrance channel region is indicated.

Fig. 2. The asymptotic electronic structure of the six potential energy surfaces arising from NO $^2\Pi$ plus NH $^3\Sigma^-$ and NH $^1\Delta$.

Fig. 3. Potential energy curves for the lowest six potential energy surfaces for NH + NO as a function of R with the other geometrical parameters fixed (See the figure inset.).

Potential Energy Surface for NH + NO

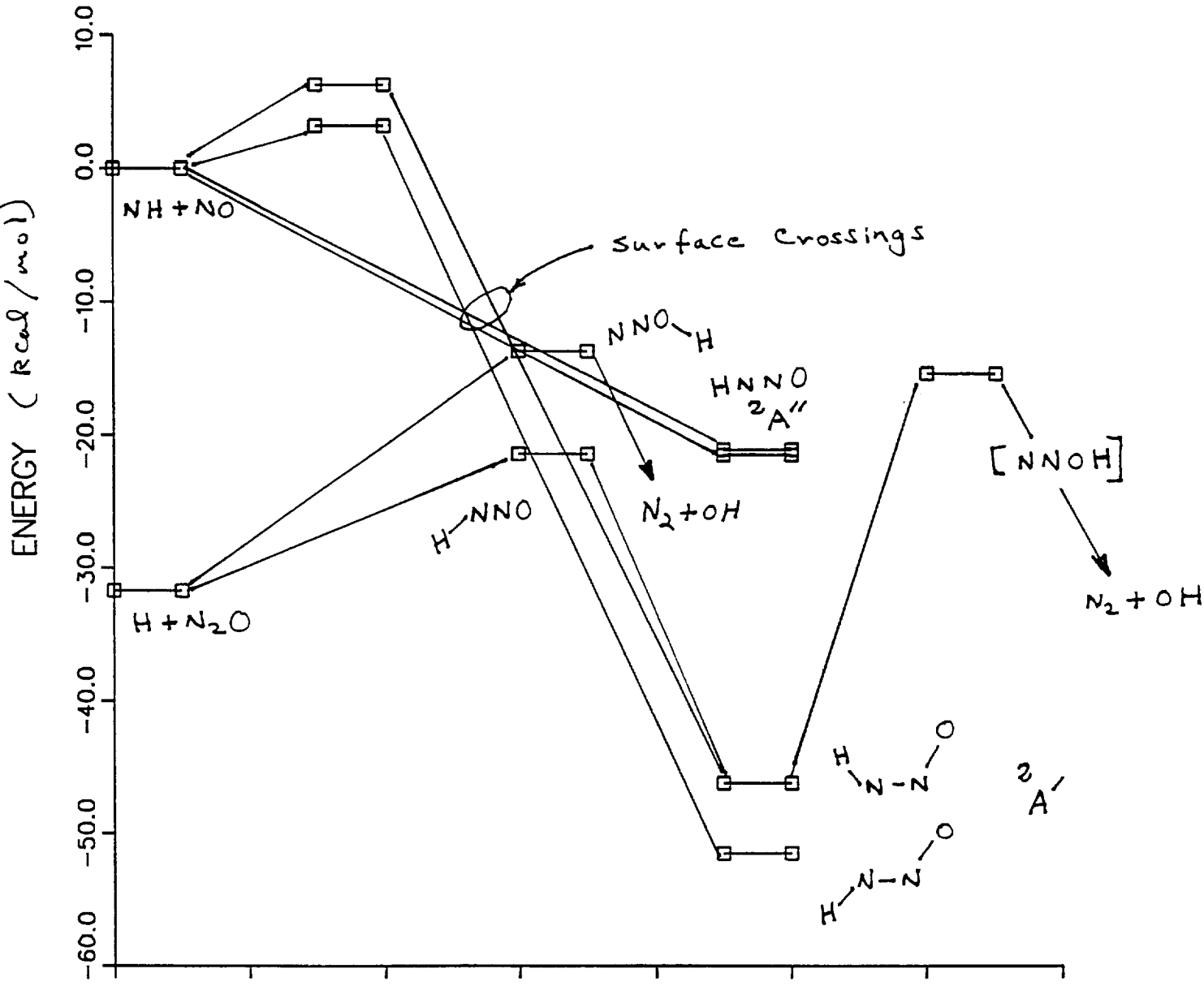

Fig. 2

NH + NO excited state surfaces

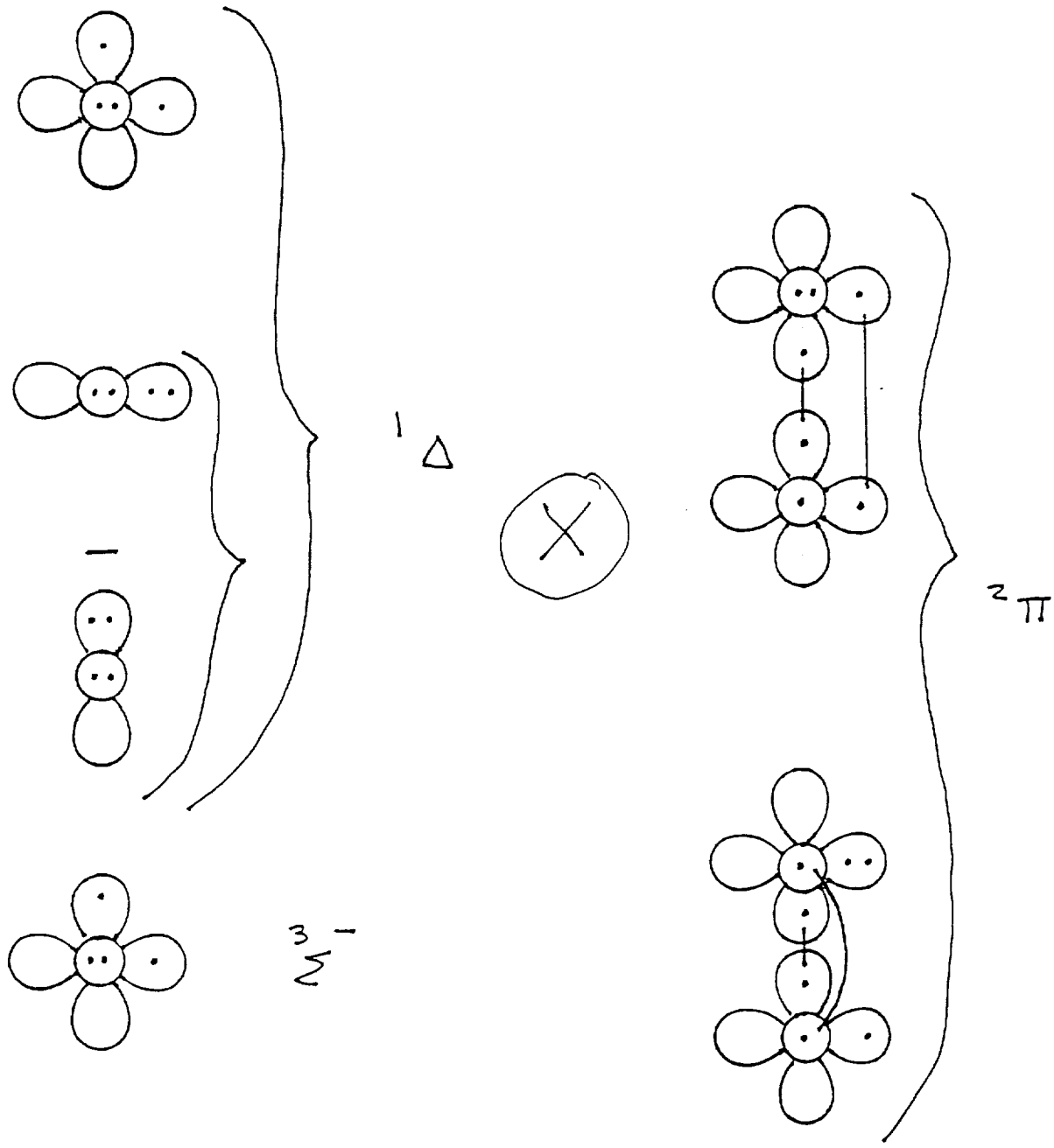

Fig. 32

State averaged CASSCF results

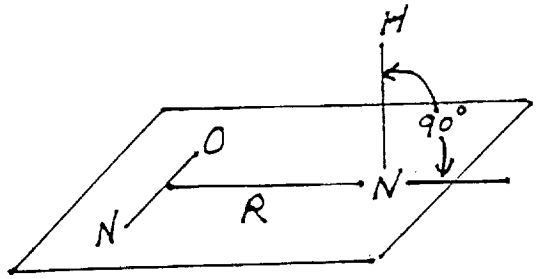

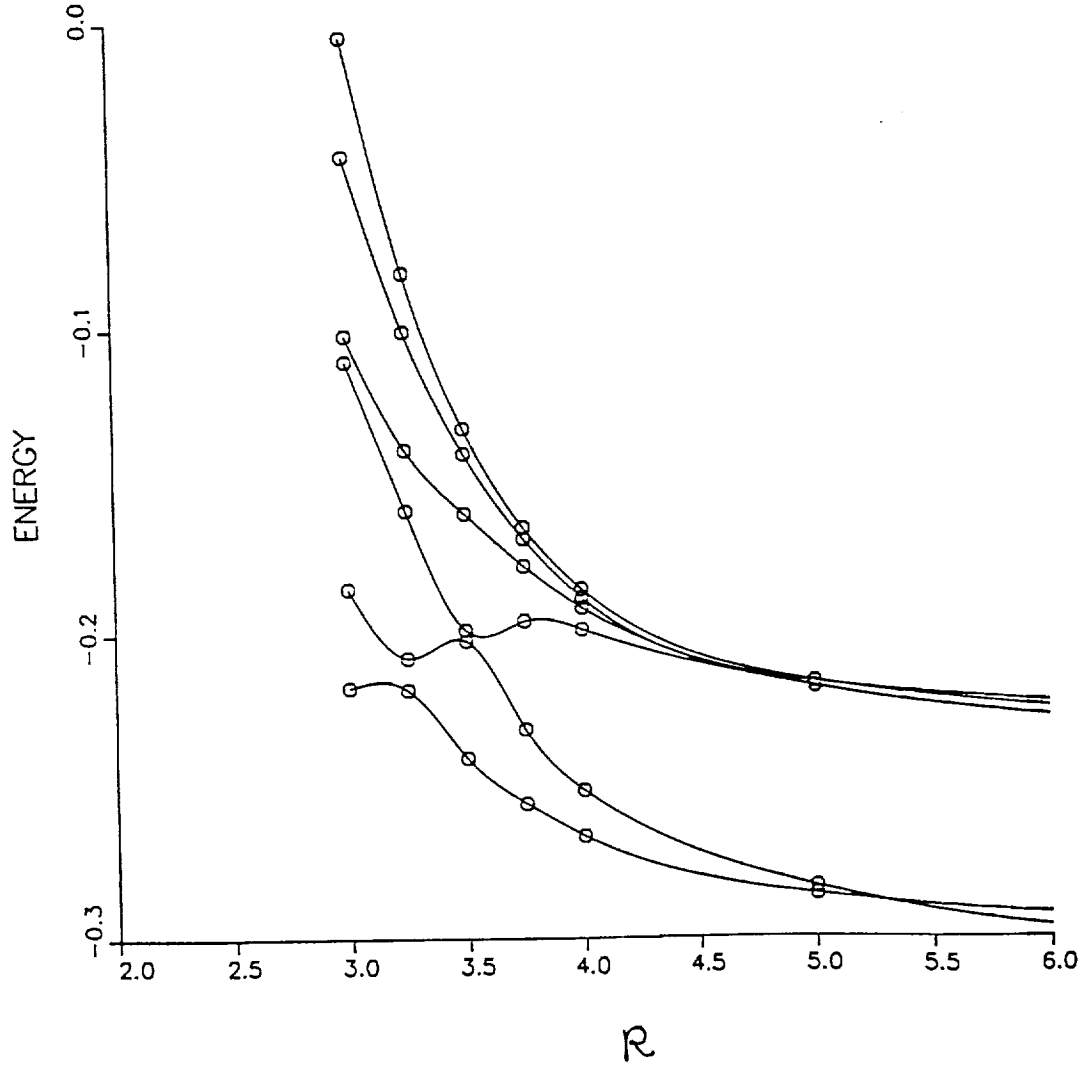

Draft date July 29, 1992
To be submitted for publication in J. Chem. Phys.

A global potential energy surface for ArH_2

David W. Schwenke,
NASA Ames Research Center, MS 230-3, Moffett Field, CA 94035-1000

Stephen P. Walch* and Peter R. Taylor**
ELORET Institute, Palo Alto, CA 94303

Abstract:

We describe a simple analytic representation of the ArH_2 potential energy surface which well reproduces the results of extensive *ab initio* electronic structure calculations. The analytic representation smoothly interpolates between the dissociated H_2 and strong bonding limits. In the fitting process, emphasis is made on accurately reproducing regions of the potential expected to be important for high temperature (*ca.* 3000 K) collision processes. Overall, the anisotropy and H_2 bond length dependence of the analytic representation well reproduce the input data.

* Mailing address: NASA Ames Research Center, MS 230-3, Moffett Field, CA 94035-1000

** Current address: San Diego Supercomputer Center, P.O. Box 85608, San Diego, CA 92186-9784

I. Introduction

In this paper we present a new potential energy surface (PES) for ArH_2. This PES is specifically tailored for use in high temperature (*ca.* 3000 K) energy transfer studies involving dissociation and recombination of H_2. This potential will be used to help understand the recombination process

$$H + H + M \rightarrow H_2 + M.$$

The recombination rates for M = H_2 [1], Ar [2] and H_2O [2] have been computed as a function of temperature using potential energy surfaces from the literature [3-5]. The result is that within a factor of 1.4 over the temperature range 1000 - 5000 K, the recombination rate is independent of the third body M. This contrasts with the prevailing experimental interpretation [6] which assigns the efficiencies 5:1:0.3 for H_2O, H_2 and Ar at 2000 K. There are several potential sources for this disagreement: inaccuracies in the potential energy surfaces used, limitations in the dynamics/kinetics calculations (see Ref.[1] for a description of the techniques we use to compute the recombination rate given a PES), or experimental uncertainties. Certainly of the three third bodies, the PES for M=Ar was the least well known. In this paper we give a PES of comparable quality to the potential energy surfaces for the other third bodies we have studied.

When constructing a PES, many different strategies are possible. One can combine data from various sources, both theoretical and experimental, and attempt to produce a function which reproduces this information. This procedure is hampered by the possibilities of inconsistency between the various input data. An alternate approach, which is used here, is to just consider data from one source, namely high quality *ab initio* electronic structure calculations. This strategy can be criticized in that certain features of the PES, such as the weak van der Waals minimum, are obtainable more easily from experimental analysis than from theoretical calculations. However, in our opinion, this drawback is more than counterbalanced by the consistency of the input data which should give rise to a PES which may more accurately reflect the shape of the accurate PES over wide regions of configuration space. We also anticipate that the features of the PES likely to be given most accurately by the electronic structure calculations, namely regions of moderate repulsion, will be predominately responsible for governing the outcome of the high temperature energy transfer processes which are of primary interest to us.

In fitting a PES for which a wide range of different interactions are possible, one has to choose between a simple function which can be expected to be accurate only in the mean or a more complicated function with many parameters. For a simple function, it is often easy to ensure that it is well behaved in extrapolated regions, while for more complicated functions it may be very difficult to ensure that extrapolation to geometries not included in the fitting procedure will give rise to physically reasonable results. In the present work we begin by using a very simple function to represent the Ar + H_2 interaction and then carefully modify it to ensure that it is well behaved globally yet accurately reproduces the input data. This is achieved using only eight parameters optimized to fit 71 energy points.

II. Electronic structure calculations.

The Ar basis set starts with a (17s12p6d4f) primitive set. The two outermost s, p, and d and the outermost f primitives are left uncontracted and the inner functions are contracted using an atomic natural orbital (ANO) scheme [7] to [5s4p2d1f]. In addition a (2s2p1d1f) set of even tempered diffuse functions is added. The resulting basis is denoted as [5+1+1s 4+1+1p 2+1+1d 1+1f] + (2s2p1d1f).

The H basis set starts with a (8s6p4d) primitive set. The outermost s and p primitives are left uncontracted and the inner functions are contracted based on ANO's to [3s2p1d]. This basis is denoted as [3+1s 2+1p 1d].

The energy calculations were designed to give an accurate description of the process H + H + Ar $\rightarrow$ H_2 + Ar. The most important nondynamical electron correlation effects were taken into account by means of complete active space, self consistent field (CASSCF) calculations, and the dynamical correlation effects were estimated using the approximately size-extensive averaged coupled pair functional (ACPF)[8] method. The CASSCF configurations correspond to a single configuration description of Ar and a two-electron two active orbital description of H_2. The full CASSCF reference space was used in the ACPF calculations. All calculations were carried out using the MOLECULE-SWEDEN [9] program system on the Ames Research Center Advanced Computation Facility CRAY Y-MP/864.

The ANO basis for H_2 was optimized at the equilibrium bond length (R_e) [7]. This makes the basis set superposition error much smaller at R_e than at other H_2 bond lengths. To help correct for this systematic error, we corrected all our energies by means of the Boys and Bernardi function counterpoise method[9.1]. Specifically,

we computed the following energies:

$E^{ArH_2}(G)$, the energy of the ArH_2 supermolecule at the ACPF level at geometry G,

$E^{H_2}(G)$, the energy of the H_2 molecule at the all single and double excitation configuration interaction (SDCI) level at geometry G including the Ar one-electron basis functions,

$E^{Ar}(G)$, the energy of the Ar atom at the ACPF level at geometry G including the H atom one-electron basis functions.

Let G^∞ be a geometry approximating Ar not interacting with H_2 but having the same H_2 bond length as in geometry G. In practice, not interacting means any two atom-atom distances greater than 30 a_0. Then we take the energy of interaction between Ar and H_2 to be

$$E^{int}(G) = E^{ArH_2}(G) - E^{ArH_2}(G^\infty) + E^{H_2}(G^\infty) - E^{H_2}(G) + E^{Ar}(G^\infty) - E^{Ar}(G). \quad (1)$$

It should be noted that, since the SDCI and ACPF methods are not exactly size-extensive, it is important to use Eq.(1) rather than $E^{ArH_2}(G) - E^{H_2}(G) - E^{Ar}(G)$ to compute the interaction energy since $E^{ArH_2}(G^\infty) \neq E^{Ar}(G^\infty) + E^{H_2}(G^\infty)$.

In Tables I and II we give the values of E^{int} computed in the course of this work. The geometries are specified by the Jacobi coordinates r, R, and χ, where r is the distance between the Ar and the center of mass of the H_2, R is the H_2 bond length, and χ is the Ar–center of mass H_2 – H angle.

III. Fitting the PES

We will optimize the parameters ($\vec{P}$) in our fitting function $[V^{int}(G, \vec{P})]$ by minimizing the least squares function

$$\phi(\vec{P}) = \sum_i \left\{ [E^{int}(G_i) - V^{int}(G_i, \vec{P})]/w_i \right\}^2. \quad (2)$$

An important aspect of the present work is the choice of the weights w_i. Previous work [10] has shown strong correlations between the force along the diatom bond evaluated at the classical turning point for relative translation and vibrational energy transfer rates, thus we wish to concentrate our interest to regions where $V^{int} \sim E_{rel}$. At 3000 K, $k_B T = 10^{-2}\ E_h$. Also $\omega\hbar$ for H_2 is about $2 \times 10^{-2}\ E_h$, so we want to focus in most closely on energies in the range $5 - 50\ mE_h$. We will

identify the weights as an acceptable error in the fit for each point. In the most interesting region, a 5% error is reasonable, thus we take

$$w_i = \max \begin{cases} \left\{0.0375\left[\log|V^{int}(G_i)/E_{\rm h}| + 2\right]^2 + 0.05\right\}|V^{int}(G_i)| \\ 10^{-4}E_{\rm h}. \end{cases} \tag{3}$$

This is a parabola in % error as a function of the order of magnitude of the energies, centered on $10{\rm m}E_{\rm h}$, except at very weakly interacting geometries, where we let the acceptable error be as large as $0.1{\rm m}E_{\rm h}$. With this weighting scheme, reporting the root mean square deviation between the fit and the input data is not meaningful — the important quantity is $\phi(\vec{P})$, which is unitless. A value equal to one means that on the average, we have attained our goal in fitting the points.

The first step in our fitting process is the determination of an ArH potential curve, $V^{\rm ArH}$. We will use this in a zeroth order representation of the ArH_2 interaction energy, *i.e.*

$$V^{int} = V^{\rm ArH}(R_+) + V^{\rm ArH}(R_-), \tag{4}$$

where $R_\pm$ are the two ArH distances, *i.e.*

$$R_\pm = \left[r^2 + (R/2)^2 \pm rR\cos\chi\right]^{\frac{1}{2}}. \tag{5}$$

This simple form will give physically reasonable results for all geometries provided $V^{\rm ArH}$ is well behaved. We choose to parameterize the potential curve as

$$V^{\rm ArH}(X) = A\exp[-bX] - \frac{C_6^{\rm ArH}}{X^6 + d^6} - \frac{C_8^{\rm ArH}}{(X^4 + d^4)^2} - \frac{C_{10}^{\rm ArH}}{(X^2 + d^2)^5}, \tag{6}$$

where $C_6^{\rm ArH} - C_{10}^{\rm ArH}$ are taken from Ref.[11]. The three parameters A, b, and d are determined by nonlinear least squares using the weights of Eq.(3) and the data given in Table I. The final value of ϕ for this fit is 0.23 with maximum weighted difference of 0.45. The final values of the fitting parameters are given in Table III where they are labeled A_0, b_0 and d_0. With these parameters, $V^{\rm ArH}$ is well behaved for all atom-atom distances.

We now turn to geometries where the two H atoms are interacting with the Ar. We start with the simple sum of pairwise interactions, Eq.(4). This simple form has several deficiencies. We correct for these deficiencies by introducing additional

dependence on the coordinates r, R, and χ other than that implicit in Eq.(5). In introducing the additional coordinate dependence, one has considerable flexibility. However, since in the limit R goes to ∞, Eq.(4) is exact, we require that the corrections to Eq.(4) vanish in this limit. The easiest way to enforce this limit is to have the corrections depend only on R and not on r or χ. We thus considered an intermediate step in the fitting process, namely fitting the *ab initio* data for fixed bond lengths. This will yield parameters fully optimized as a function of R. In the final step, we will fit the dependence of the parameters on R. The intermediate step involves fewer points and parameters than the final step and provides excellent initial guesses for nonlinear parameters. It will also tell us whether or not it is possible to obtain a satisfactory fit with only R dependent parameters. In the present case, we will see that it will be possible to obtain accurate fits with this restriction.

The first correction to Eq.(4) concerns the long range attractive term. The leading contribution from $C_6^{\mathrm{ArH}}/(R_\pm^6 + d^6)$ expanded in terms of the Jacobi coordinates is $2C_6^{\mathrm{ArH}}/r^6 + O(r^{-8})$ which can be compared with the more accurate form $C_6^{\mathrm{ArH_2}}(R)[1 + \Gamma_6^{\mathrm{ArH_2}}(R)P_2(\cos\chi)]/r^6 + O(r^{-8})$. Our hypothesis requires that we neglect the P_2 term, however this is not a bad approximation since $\Gamma_6^{\mathrm{ArH_2}}(R) \sim 10\%$ for R near R_e [13]. We thus scale the long range part of Eq.(4) by the factor $g(R) = C_6^{\mathrm{ArH_2}}(R)/2C_6^{\mathrm{ArH}}$ and we fit the data of Varandas [13] to $g(R) = \{\beta \exp[-\alpha(R - R_0)] + 1\}^{-1}$ with $\alpha = 2\ a_0^{-1}$, $\beta = 0.437$ and $R_0 = 1.449 a_0$. As R becomes large, $g(R)$ becomes unity and we recover the ArH long range interaction.

The next deficiency we address is the anisotropy of the sum of pairwise interactions, *e.g.* the χ dependence. Using Eq.(4) with the scaled long range potential results in too much anisotropy. We interpret this as a manifestation of the migration of charge density toward the center of the H_2 bond, thus we introduce the shift ρ, *i.e.* we replace $R_\pm$ in Eq.(5) with

$$\tilde{R}_\pm = \left[r^2 + \left(\frac{R-\rho}{2}\right)^2 \pm r(R-\rho)\cos\chi\right]^{\frac{1}{2}}, \tag{7}$$

thus we take

$$V^{int}(r,R,\chi,A,b,d,\rho) = A\big[\exp(-b\tilde{R}_+) + \exp(-b\tilde{R}_-)\big]$$
$$- g(R)\big\{C_6^{\rm ArH}\big[(\tilde{R}_+^6 + d^6)^{-1} + (\tilde{R}_-^6 + d^6)^{-1}\big] + C_8^{\rm ArH}\big[(\tilde{R}_+^4 + d^4)^{-2} + (\tilde{R}_-^4 + d^4)^{-2}\big]$$
$$+ C_{10}^{\rm ArH}\big[(\tilde{R}_+^2 + d^2)^{-5} + (\tilde{R}_-^2 + d^2)^{-5}\big]\big\}. \tag{8}$$

Finally we optimize the four parameters A, b, d, and ρ for each value of R. The value of ϕ for each value of R is given in Table IV under the column marked optimum. A satisfactory fit is obtained for all H_2 bond lengths.

To complete our fit, we must parameterize $A(R)$, $b(R)$, $d(R)$, and $\rho(R)$. We first consider $\rho(R)$. Since this parameter is based upon the idea of charge flow, we will tie it to a molecular property which reflects this, namely the quadrupole moment. Specifically we take

$$\rho(R) = R\Big\{1 - \big[1 + q(R)/\delta R^2\big]^{-\frac{1}{2}}\Big\}, \tag{9}$$

where $q(R)$ is the quadrapole moment of H_2. We will use the fit of Ref.[3] to generate $q(R)$ at all R. This contains the single parameter δ. Originally, we tried to parameterize $\rho(R)$ as the displacement of a fixed point charge required to reproduce $q(R)$, but we were not successful. Equation (9) represents the displacement required to reproduce $q(R)$ for a R dependent point charge with R dependence leading to a constant discriminant in the quadratic equation for which $\rho(R)$ is a root.

The remaining functions are represented as an expansion in terms of even tempered exponentials, *i.e.*

$$X(R) = \sum_{i=0}^{i_{\max,X}} X_i[-\exp(\alpha_X R)]^i, \tag{10}$$

where $X = A$, b, or d, with the $i = 0$ coefficient fixed by the fit to the ArH interaction. In our final fit we use $i_{\max,A} = 2$ and $i_{\max,b} = i_{\max,d} = 1$. The parameters for the fit are given in Table III and the weighted errors as a function of R in Table IV. The maximum weighted error is 2.7 and the number of geometries with weighted errors greater than one is five. With these parameters, the fit seems to be globally well behaved.

IV. Discussion

We first consider the ArH interaction. The fit is quite good, however it does not well reproduce the empirical ArH potential from Ref.[11]. See Fig. 1. The present ArH potential curve has van der Waals minimum parameters $R_{\rm min} = 7.13\ a_0$ $V_{\rm min} = -0.102\ {\rm m}E_{\rm h}$ compared to $R_{\rm min} = 6.68\ a_0$ $V_{\rm min} = -0.175\ {\rm m}E_{\rm h}$ for the Tang-Toennies potential including up to C_{18}. The Tang-Toennies potential is also much more repulsive at distances less than $R_{\rm min}$. The reason for this discrepancy is not clear, for improving the theoretical calculations by both expanding the one-electron basis set and changing the electron correlation treatment does not significantly change the present result [12].

We can also compare to empirically determined values of the functions in the expansion

$$V^{int}(r, R = 1.449\ a_0, \chi) = v_0(r) + P_2(\cos\chi)v_2(r) \tag{11}$$

given in Ref. [14]. This is done in Fig. 2 where we also give v_0 and v_2 computed from the *ab initio* data and the current fit. These functions for the fit do not change significantly between $R = 1.401$ and $R = 1.449$, so it is meaningful to compare the functions for the two distances. The comparison between the v_0 term is very similar to the ArH potential: the fit well reproduces the *ab initio* data and the minimum for the Tang-Toennies function is deeper and closer in: $R_{\rm min} = 6.77\ a_0$ and $V_{\rm min} = -0.232\ {\rm m}E_{\rm h}$ versus $R_{\rm min} = 7.10\ a_0$ and $V_{\rm min} = -0.157\ {\rm m}E_{\rm h}$ for the fit. In contrast, for the v_2 term, the Tang-Toennies function fits the *ab initio* data better than the fit in the well region. The failure of the fit to reproduce the *ab initio* result is presumably due to the fact that the leading long range anisotropic contribution is proportional to r^{-8}. However, since v_2 is not large, the absolute magnitudes of the deviations are not large.

Now consider the consequence of stretching the H_2 bond. The most interesting orientation to consider is that for $\chi = \pi/2$, the T-shaped geometries. In Fig. 3 we compare the fit to the *ab initio* data for repulsive geometries. On the whole we see very good agreement between the fit and the data. This particular orientation is interesting because the *ab initio* data and the fit predict that at R_e, V^{int} will increase as R increases whereas a simple pairwise additive model would give the reverse trend. It is the inclusion of the R dependent shift $\rho(R)$ which is primarily responsible for the correct sign of the slope for the present fit. Eventually as R increases, the slope changes sign and the fit appears to do a reasonable job at predicting the position of the sign change. However, in this figure, larger deviations appear for

$R = 3$ than for the other geometries. This is also shown by the weighted errors in Table IV. This is probably an indication that a more sophisticated treatment of the anisotropy is required.

In the course of the present work we considered several variants of the present fit. All of these were attempts to improve the description of the anisotropy of the PES. An obvious place to start is to replace the function $g(R)$ used to scale the dispersion terms with the function of Ref.[13] which includes χ dependence and a more accurate R dependence. We also considered introducing $P_2(\cos\chi)$ anisotropy into the functions $A(R)$, $b(R)$, $d(R)$ and $\delta(R)$. By doing so, it was possible to substantially reduce the weighted errors for $R = 1$ and 1.401, but the improvement for $R = 3$ and 5 was much more modest. These fits also yielded more complicated R dependence for $A(R)$ etc and so it was very hard to produce functions which gave rise to a globally well behaved PES. On the whole, the present fit was outstanding in its ability to accurately predict the global shape of the PES.

IV. Conclusions

In this paper we have presented a simple yet accurate function to interpolate/extrapolate the interaction energy of Ar+H_2. In conjunction with an accurate H_2 potential curve, such as that from Ref.[3], this defines a global PES suitable for studying energy transfer and dissociative collisions. The function does not well reproduce empirical estimates of the van der Waals well region, but does reproduce reasonably well the *ab initio* data in that region. The force along the H_2 bond is well represented globally without recourse to switching functions.

V. Acknowledgements

SPW is supported by NASA grant no. NCC2-478 and PRT is supported by NASA grant no. NCC2-371.

References.

1. D. W. Schwenke, J. Chem. Phys. **92**, 7267 (1989).
2. D. W. Schwenke, unpublished calculations.
3. D. W. Schwenke, J. Chem. Phys. **89**, 2076 (1988).
4. N. C. Blais and D. G. Truhlar, J. Chem. Phys. **65**, 5335 (1976).
5. D. W. Schwenke, S. P. Walch, and P. R. Taylor, J. Chem. Phys **94**, 2986 (1991).
6. N. Cohen and K. R. Westberg, J. Phys. Chem. Ref. Data **12**, 531 (1983).
7. J. Almlöf and P. R. Taylor, J. Chem. Phys. **86**, 4070 (1987).
8. R. J. Gdanitz and R. Ahlrichs, Chem. Phys. Lett. **143**, 413 (1988).
9. MOLECULE-SWEDEN is an electronic structure program system written by J. Almlöf, C. W. Bauschlicher, M. R. A. Blomberg, D. P. Chong, A. Heiberg, S. R. Langhoff, P.-Å. Malmqvist, A. P. Rendell, B. O. Roos, P. E. M. Siegbahn, and P. R. Taylor.

9.1 S. F. Boys and F. Bernardi, Mol. Phys. **19**, 553 (1970).

10. D. W. Schwenke and D. G. Truhlar, J. Chem. Phys. **81**, 5586 (1984).
11. K. T. Tang and J. P. Toennies, Chem. Phys. **156**, 413 (1991).
12. H. Partridge, unpublished calculations.
13. A. J. C. Varandas and M. A. Matías, Chem. Phys. Lett. **148**, 149 (1988).
14. K. T. Tang and J. P. Toennies, J. Chem. Phys. **74**, 1148 (1981).

Table I. ArH interaction energies.

$R_{\mathrm{ArH}}(a_0)$	E^{int} (mE_h)	V^{ArH} (mE_h)
2.	215.740	205.625
3.	50.853	49.295
4.	11.278	11.505
5.	1.912	1.885
6.	0.119	0.110
7.	-0.095	-0.101
8.	-0.072	-0.078
9.	-0.040	-0.044
10.	-0.021	-0.024

Table II. ArH_2 interaction energies.

	E^{int} (mE_h)			
$r(a_0)$	$R = 1\ a_0$	$R = 1.401$	$R = 3$	$R = 5$
		$\chi = 0$		
3.	158.061	182.810	535.157	[a]
4.	25.707	32.480	73.251	522.077
5.	3.202	4.546	16.575	90.337
6.	0.089	0.219	2.757	22.709
8.	-0.094	-0.129	-0.218	0.533
10.	-0.025	-0.035	-0.082	-0.103
		$\chi = \pi/4$		
3.	144.256	154.744	151.256	150.373
4.	23.772	28.272	41.471	62.092
5.	2.981	3.937	8.873	18.126
6.	0.098	0.190	1.175	4.016
8.	-0.082	-0.112	-0.185	-0.088
10.	-0.020	-0.031	-0.062	-0.068
		$\chi = \pi/2$		
3.	133.271	136.783	97.310	29.719
4.	22.015	24.734	23.799	8.183
5.	2.765	3.404	4.233	1.444
6.	0.097	0.164	0.340	-0.016
8.	-0.077	-0.097	-0.145	-0.119
10.	-0.021	-0.027	-0.045	-0.037

[a] Very repulsive so not computed.

Table III. ArH_2 PES parameters (in atomic units).

X	X_0	X_1	X_2	α_X
A	18.06	58.63	-90.61	0.7662
b	1.653	0.3874		0.7662
d	2.339			
			$\delta = 0.2369$	

Table IV. Root mean square errors for ArH_2 PES fit.

R	Optimum	Fit
1.0	0.20	0.32
1.401	0.29	0.46
3.0	0.85	0.98
5.0	0.55	0.82
all	0.54	0.70

Figure captions:

Figure 1: The ArH potential curve from *ab initio* calculations (symbols), from the present fit , Eq. (6) (solid line), and from Tang and Toennies [11]. Note the switch between a linear and log scale at 0.1 mE_h.

Figure 2: The first two terms in a Legendre expansion of the ArH_2 PES. Circles, v_0 from *ab initio* points; squares v_2 from *ab initio* points; solid line fit; dashed line, the fit of Tang and Toennies [14]. Note the switch between a linear and log scale at 0.1 mE_h.

Figure 3: The dependence of the potential energy on the H_2 bond length for $\chi = \pi/2$. The symbols are the *ab initio* points with squares for $r = 3$ a_0, circles for $r = 4$, triangles for $r = 5$, and crosses for $r = 6$. The solid lines are the fit at the corresponding values of r.

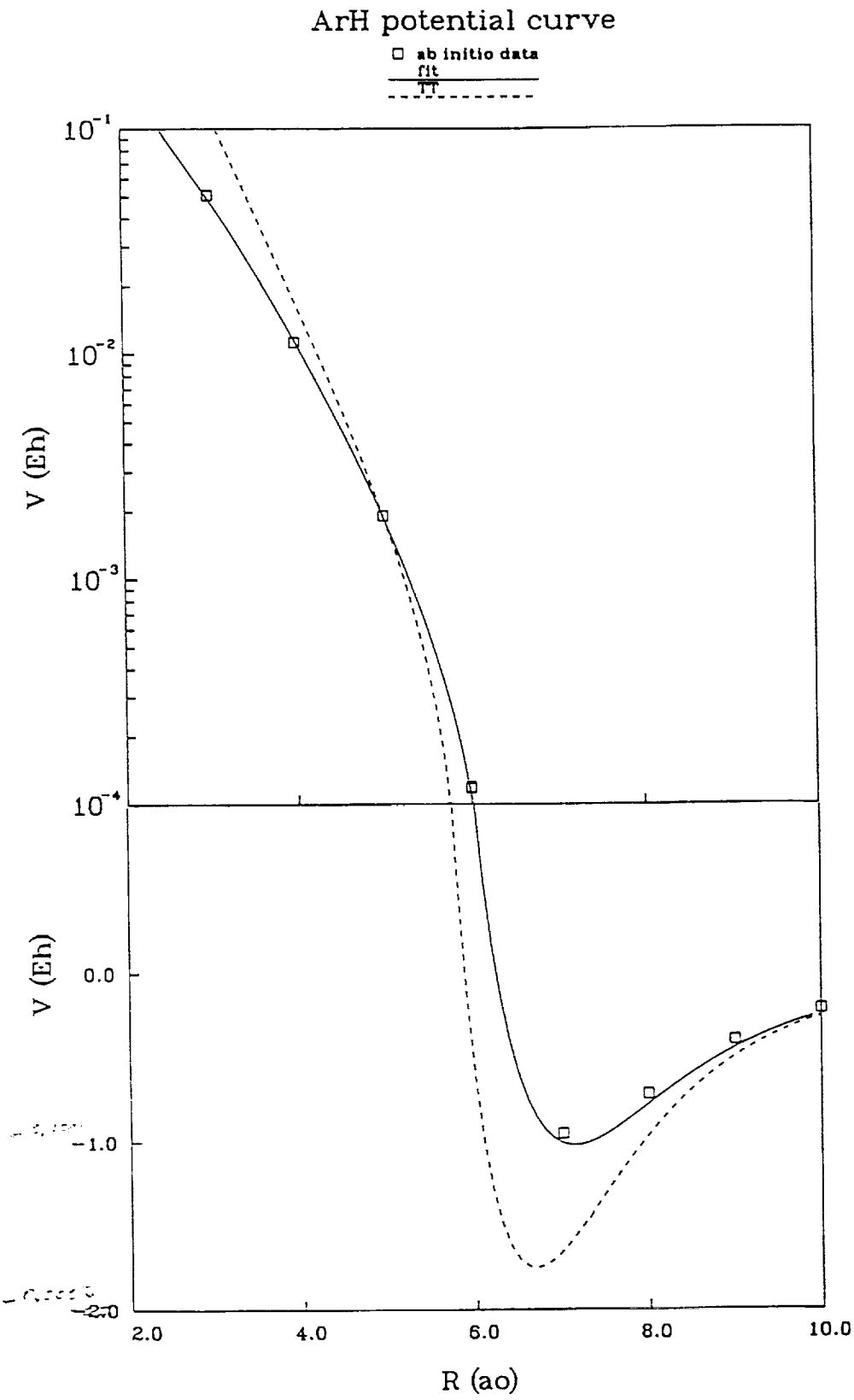
ArH potential curve
ab initio data
fit
TT
V (Eh)
10^{-1}
10^{-2}
10^{-3}
10^{-4}
V (Eh)
0.0
−1.0
−2.0
2.0
4.0
6.0
8.0
10.0
R (ao)

fig. 1

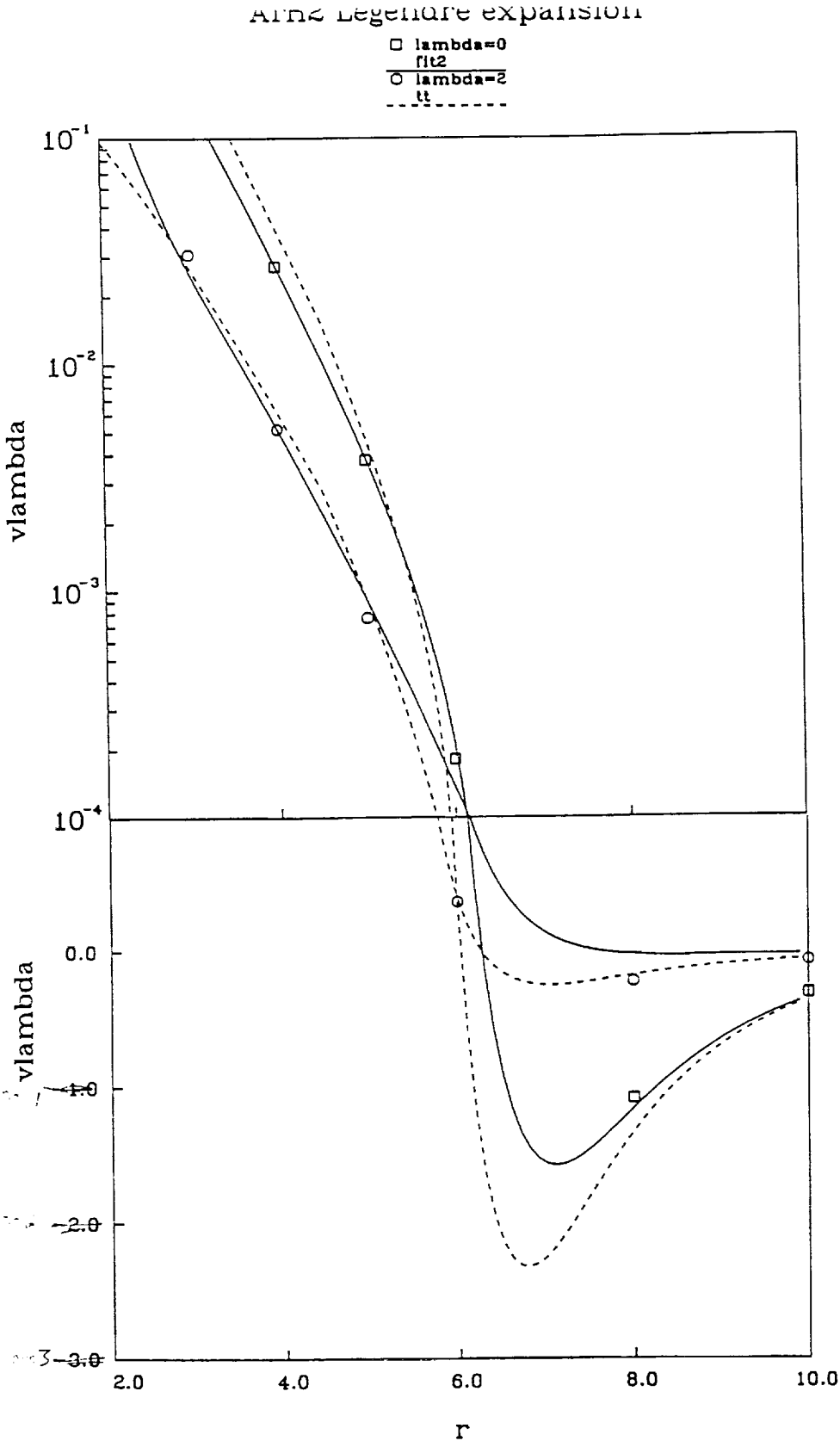
AFH2 Legendre expansion
lambda=0
fit2
lambda=2
tt
vlambda
vlambda
r
10^{-1}
10^{-2}
10^{-3}
10^{-4}
0.0
-1.0
-2.0
-3.0
2.0
4.0
6.0
8.0
10.0

fig. 2

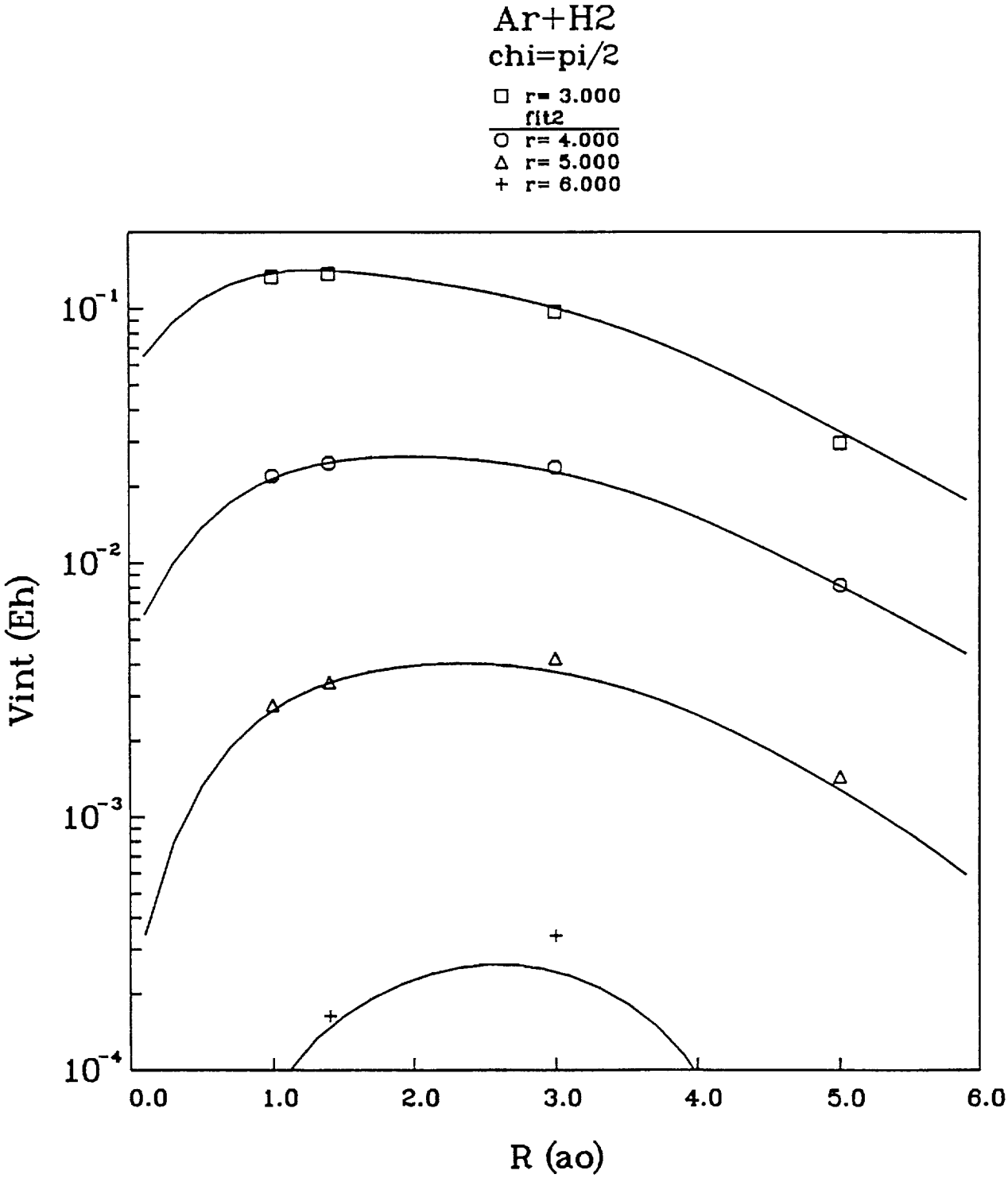
Ar+H2
chi=pi/2
r= 3.000
fit2
r= 4.000
r= 5.000
r= 6.000
Vint (Eh)
10^-1
10^-2
10^-3
10^-4
0.0
1.0
2.0
3.0
4.0
5.0
6.0
R (ao)

fig. 3